Inorg. Chem. **2003**, *42*, 7489–7501

Syntheses, Spectroscopy, and Redox Chemistry of Encapsulated Oxo–Mo(V) Centers: Implications for Pyranopterin-Containing Molybdoenzymes

Partha Basu,* Victor N. Nemykin, and Raghvendra S. Sengar

Department of Chemistry and Biochemistry, Duquesne University, Pittsburgh, Pennsylvania 15282

Received July 14, 2003

Coordination by at least four sulfur donors to an embedded molybdenum center has been found to be a common feature in the crystal structures of many mononuclear molybdenum enzymes. In an effort to model embedded molybdenum centers, we have synthesized dendritic thiolate ligands and their oxo–molybdenum complexes containing a $[Mo^{V}OS_4]^-$ core. These compounds have been isolated in pure form as blue solids or gummy materials, and the molecular nature of these compounds has been confirmed by electrospray ionization mass spectrometry and infrared, electron paramagnetic resonance, and UV–vis spectroscopies. The dendritic complexes exhibit little variation in their broad S → Mo charge transfer band ($\lambda_{max} \sim 600$ nm; $\epsilon \sim 6000$ M^{-1} cm^{-1}), Mo═O vibration energy (941–943 cm^{-1}), and EPR *g*-values ($g_{||} \sim 2.02$; $g_{\perp} \sim 1.98$; $g_{av} \sim 1.99$). The spectroscopic data confirm the integrity of the square pyramidal $[Mo^{V}OS_4]^-$ core with little geometric distortions, suggesting that the electronic structure at the metal center is not perturbed by the ligand architecture. The electronic structure of these complexes, calculated by the density functional theory, demonstrates a similar composition of the HOMO. In complexes **6** and **7a**, the energy of the HOMO orbital might be modulated by the difference in the electronic structure of the ligands. The Mo(V/IV) reduction potentials vary as a function of the dielectric constant and the donor number of the solvent. The kinetics of the reduction is influenced by the reorganization of the geometry and the encapsulating effect. We suggest that protein structure imposed microenvironments may control the dielectric properties and hence the redox properties of the metal center in many metallobiomolecules.

Introduction

Mononuclear molybdenum containing enzymes catalyze a wide variety of reactions such as the reduction of nitrate to nitrite, reduction of dimethyl sulfoxide to dimethyl sulfide, reduction of arsenate to arsenite, or the oxidation of sulfite to sulfate.[1−3] These reactions play critical roles in the global cycling of elements such as nitrogen, sulfur, carbon, and arsenic. The catalytic reactions take place at the molybdenum center, which is coordinated by the ene-dithiolate moiety of one or two pyranopterin cofactors (Figure 1). Hille[3] classified these enzymes into three distinct families: xanthine oxidase family, sulfite oxidase family, and dimethyl sulfoxide reductase (DMSOR) family; representative members of each family have now been crystallographically characterized. Using the inferred sequences and known biochemistry, the nitrate reductases have been classified, and on the basis of a detailed sequence analysis, the evolutionary lineages among these enzymes have been proposed.[4]

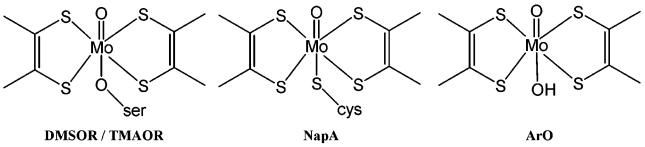

Figure 1. Structure of the cofactor and coodination environment of dimethyl sulfoxide reductases (DMSOR), trimethylamine *N*-oxide reductases (TMAOR), periplasmic nitrate reductases (NapA), and arsenite oxidase (ArO).

The members of the DMSO reductase family are prokaryotic enzymes in which the molybdenum centers are coordinated by two pyranopterin cofactors as confirmed crystallographically. For example, in the crystal structures of dissimilatory nitrate reductase (i.e., NapA) from

* To whom correspondence should be addressed. E-mail: basu@duq.edu.

(1) Enemark, J. H.; Young, C. G. *Adv. Inorg. Chem.* **1993**, *40*, 1−88.
(2) Zumft, W. G. *Microbiol. Mol. Biol. Rev.* **1997**, *61*, 533−615.
(3) Hille, R. *Chem. Rev.* **1996**, *96*, 2757−2816.
(4) Stolz, J. F.; Basu, P. *ChemBioChem* **2002**, *3*, 198−206.

10.1021/ic034821r CCC: $25.00
Published on Web 10/24/2003

Desulfovibrio desulfuricans, the molybdenum center is coordinated by two ene-dithiolates of two pyranopterin cofactors and one cysteinato sulfur atom.[5] The presence of two pyranopterin cofactors per molybdenum atom has also been confirmed in the crystal structures of DMSOR from *Rhodobacter sphaerodies*[6] and *R. capsulatus*,[7,8] trimethylamine oxide reductase (TMAOR) from *Shewanella massilia*,[9] arsenite oxidase from *Alcaligenes faecalis*,[10] and formate dehydrogenases (FDH-H and FDH-N) from *Escherichia coli*.[11] Additional coordination from the protein side chain to the molybdenum atom is provided by a serinato oxygen in DMSOR[6−8] and TMAOR,[9] and by selenocysteine in FDH,[11] while in arsenite oxidase no amino acid coordinates the molybdenum center. Thus, a molybdenum center coordinated by four sulfur donors emerges as the minimal motif in members of the DMSOR family. On the basis of the structural studies of enzymes such as NapA[5] and DMSOR from *R. sphaerodies*,[6] it has been proposed that the desoxo−molybdenum(IV) center is the catalytically competent state, and in the fully oxidized state, the metal center is coordinated by a single terminal oxo group. The high-resolution structure of DMSOR exhibited a disordered (between penta- and hexacoordinated forms) active site.[6b] In addition, structural studies have demonstrated that the molybdenum centers are buried within the protein matrix, and as such the coordinating ligands are not exposed to the surface. They are, however, associated with either a channel or a crevice presumably for substrate entrance and product release.

During the course of catalysis, the molybdenum center passes through a 5+ oxidation state, as determined by electron paramagnetic resonance (EPR),[12] magnetic circular dichroism (MCD),[13] and extended X-ray absorption fine structure (EXAFS) spectroscopies.[14−16] These studies also indicate the presence of one terminal oxo group coordinated to the metal center in the 5+ oxidation state, although a recent pulsed EPR investigation[17] suggests a Mo−OH unit as the EPR active species. Taken together, it appears that the minimal picture of molybdenum(V) centers that emerges is of a $[Mo^{V}OS_4]$ core buried inside the protein. Interestingly, when other biomimetic electroactive centers are encapsulated, such as hemes and iron−sulfur clusters, they exhibit a significant modulation in the reduction potentials.[18−20] We recently reported the synthesis of $[Mo^{V}O(p\text{-}SC_6H_4{-}R)_4]^-$ centers, where R represents a small to large organic functionality.[21] Herein we disclose the complete synthetic and spectroscopic details, and solvent dependent electrochemistry of the oxo−molybdenum complexes coordinated by dendritic thiolato ligands. Moreover, using density functional theory, we discuss the electronic structure of $[MoOS_4]^-$ cores. We also have calculated the significance of the steric encumbrance with respect to the protein chemistry.

Experimental Section

The syntheses of all molybdenum complexes were carried out in oxygen free dry argon atmosphere using dry distilled solvents either following the Schlenk techniques or inside an inert (N_2) atmosphere drybox. Syntheses of dendron **1** and **2** were carried out in air.

Materials and Supplies. Solvents were purchased either from Aldrich Chemical Co. or Acros Chemical Company and were purified before use. The solvents were purified as follows: acetonitrile (MeCN) from CaH_2 followed by Li_2CO_3−$KMnO_4$ and finally from P_2O_5; methylene chloride (CH_2Cl_2) from CaH_2; toluene and THF (THF) from Na−benzophenone; ethanol over sodium ethoxide; and 2-methoxyethanol over K_2CO_3. 4-Mercaptobenzoic acid, oxalyl chloride, dimethyl formamide (DMF), ferrocene, tetrabutylammonium perchlorate (TBAP), tetraethylammonium tetrafluoroborate, solium borohydride, and tetraphenyl phosphonium chloride were purchased from Aldrich Chemical company and were used without any purification. Silica gel (70−230 mesh) and Bio Beads SX3 were purchased from Aldrich and Biorad, respectively.

Spectroscopy and Electrochemistry. Infrared spectra were recorded on a Perkin-Elmer FT-IR 1760X spectrometer in KBr pellets or NaCl plates. The electronic spectra were recorded on a Cary 14 spectrophotometer with an OLIS 14 version 2.6.99 operating system or Cary 3 spectrophotometer connected with constant temperature circulators. Electrochemical measurements were carried out using a Bioanalytical Systems (BAS) model CV-50W. Cyclic voltammograms were recorded with a standard three-electrode system consisting of a Pt-disk working electrode, a Pt-reference electrode, and a Pt-wire auxiliary electrode. TBAP was used as the supporting electrolyte, and all voltammograms were internally referenced to ferrocene. As such, the potentials are reported with respect to the Fc^+/Fc couple, without junction correction. All cyclic voltammograms were simulated digitally to

(5) Dias, J. M.; Than, M. E.; Humm, A.; Huber, R.; Bourenkov, G. P.; Bartunik, H. D.; Bursakov, S.; Calvete, J.; Caldeira, J.; Carneiro, C.; Moura, J. J. G.; Moura, I.; Romão, M. J. *Structure* **1999**, *7*, 65−79.

(6) (a) Schindelin, H.; Kiser, C.; Hilton, J.; Rajagopalan, K. V.; Rees, D. C. *Science* **1996**, *272*, 1615−1621. (b) Li, H.-K.; Temple, C.; Rajagopalan, K. V.; Schindelin, H. *J. Am. Chem. Soc.* **2000**, *122*, 7673−7680.

(7) McAlpine, A. S.; McEwan, A. G.; Bailey, S. *J. Mol. Biol.* **1998**, *275*, 613−623.

(8) Schneider, F.; Löwe, J.; Huber, R.; Schindelin, H.; Kiser, C.; Knäblein, J. *J. Mol. Biol.* **1996**, *263*, 53−69.

(9) Czjzek, M.; Santos, J.-P. D.; Pommier, J.; Giordano, G.; Mejean, V.; Haser, R. *J. Mol. Biol.* **1998**, *284*, 435−447.

(10) Ellis, P. J.; Conrads, T.; Hille, R.; Kuhn, P. *Structure* **2001**, *9*, 125−132.

(11) (a) Boyington, J. C.; Gladyshev, V. N.; Khangulov, S. V.; Stadtman, T. C.; Sun, P. D. *Science* **1997**, *275*, 1305−1308. (b) Jormakka, M.; Tornroth, S.; Byrne, B.; Iwata, S. *Science* **2002**, *295*, 1862−1868.

(12) George, G. N.; Turner, N. A.; Bray, R. C.; Morpeth, F. F.; Boxer, D. H.; Cramer, S. P. *Biochem. J.* **1989**, *259*, 693−700.

(13) (a) Helton, M. E.; Pacheco, A.; McMaster, J.; Enemark, J. H.; Kirk, M. L. *J. Inorg. Biochem.* **2000**, *80*, 227−233. (b) Jones, R. M.; Inscore, F. E.; Hille, R.; Kirk, M. L. *Inorg. Chem.* **1999**, *38*, 4963−4970. (c) Benson, N.; Farrar, J. A.; McEwan, A. G.; Thomson, A. J. *FEBS Lett.* **1992**, *307*, 169−172. (d) Finnegan, M. G.; Hilton, J.; Rajagopalan, K. V.; Johnson, M. K. *Inorg. Chem.* **1993**, *32*, 2616−2617.

(14) Baugh, P. E.; Garner, C. D.; Charnock, J. M.; Collison, D.; Davies, E. S.; McAlpine, A. S.; Bailey, S.; Lane, I.; Hanson, G. R.; McEwan, A. G. *JBIC, J. Biol. Inorg. Chem.* **1997**, *2*, 634−643.

(15) George, G. N.; Hilton, J.; Temple, C.; Prince, R. C.; Rajagopalan, K. V. *J. Am. Chem. Soc.* **1999**, *121*, 1256−1266.

(16) George, G. N.; Hilton, J.; Rajagopalan, K. V. *J. Am. Chem. Soc.* **1996**, *118*, 1113−1117.

(17) Raitsimring, A. M.; Astashkin, A. V.; Feng, C.; Enemark, J. H.; Nelson, K. J.; Rajagopalan, K. V. *JBIC, J. Biol. Inorg. Chem.* **2003**, *8*, 95−104.

(18) Cardona, C. M.; Mendoza, S.; Kaifer, A. E. *Chem. Soc. Rev.* **2000**, *29*, 37−42.

(19) Weyermann, P.; Gisselbrecht, J.-P.; Boudon, C.; Diederich, F.; Gross, M. *Angew. Chem., Int. Ed.* **1999**, *38*, 3215−3219.

(20) Gorman, C. B.; Smith, J. C.; Hager, M. W.; Parkhurst, B. L.; Gracz, H. S.; Haney, C. A. *J. Am. Chem. Soc.* **1999**, *121*, 9958−9966.

(21) Mondal, S.; Basu, P. *Inorg. Chem.* **2001**, *40*, 192−193.

obtain the half wave potentials. Mass spectra were collected on a Micromas ZMD mass spectrometer using both negative and positive ionization modes with the electrospray ionization (ESI) source. Acetonitrile solutions of the samples were injected via a syringe pump with a flow rate of 0.1 mL/min. X-band (∼9 GHz) CW-EPR spectra were recorded on a Bruker 300 spectrometer equipped with an Oxford ESR 910 cryostat for low temperature measurement. Spectra were collected at 20 K with MeCN/toluene (50:50 v/v) as a glassy solvent. Room temperature ^{1}H (at 300 MHz) and ^{13}C (at 75.5 MHz) NMR spectra were recorded on a Bruker ACP-300 spectrometer with both $CDCl_3$ and DMSO-d_6.

Computational Details. The known crystal structure of $(AsPh_4)[MoO(SPh)_4]$[22] was used for calculating the electronic structure of $[MoO(SPh)_4]^-$. For the electronic structure calculation of $[MoO(p\text{-}SC_6H_4CONHCH_3)_4]^-$, the geometry of the $CONHCH_3$ group was optimized by the PM3(tm) method,[23] and the optimized structure was added at the para position of the thiophenyl rings of $(AsPh_4)[MoO(SPh)_4]$. For calculations on $[MoO(SPh)_4]^-$ and $[MoO(p\text{-}SC_6H_4CONHCH_3)_4]^-$cores, C_4 symmetry was adopted. In another set of calculations, the geometries of $[MoO(SPh)_4]^-$ and $[MoO(p\text{-}SC_6H_4CONHCH_3)_4]^-$cores were optimized with the LANL2DZ basis set at the same level of theory used for single-point calculations (vide infra). All semiempirical calculations, using the PM3(tm) method, were carried out using Hyperchem[24] software on a personal computer running on Windows operating system. The density functional calculations were performed using Becke's three-parameter hybrid exchange functional[25] and the Lee−Yang−Parr nonlocal correlation functional[26] (B3LYP) in the borders of unrestricted or restricted-open Hartree−Fock formalism. For DFT calculations, the molybdenum atom is described with a DGauss full electron double-ζ basis set with polarization having a (18s,12p,9d) → [6s,5p,3d] contraction scheme;[27] for all other atoms the standard 6-311G(d) basis set[28] was used. All single point and geometry optimization DFT calculations were performed using the Gaussian 98 program family[29] running on either the Windows or the Linux operating system. Time-dependent DFT (TDDFT) calculations were done using unrestricted-open shell calculations using X-ray crystallography adapted geometries of $[MoO(SPh)_4]^-$ and $[MoO(p\text{-}SC_6H_4CONHCH_3)_4]^-$ cores. A typical TDDFT calculation on the $[MoO(p\text{-}SC_6H_4CONHCH_3)_4]^-$ core using 8 processors and 1.5 GB of RAM in HITAC Risc supercomputer took nearly 80 h. The solvation and reorganization effects were calculated by using the isodensity polarized continuum model (IPCM)[30] coupled with self-consistent reaction field procedure implemented in Gaussian 98 program.[31] All calculations employed Becke's three-parameter hybrid exchange functional[25] and the gradient corrections of Perdew, along with his 1981 local correlation functional[32] (B3P86). We have chosen this functional because our calculations[33,34] as well as published data from the other laboratories[35] suggest that the geometries and thermodynamic properties calculated with the B3P86 functional are in good agreement. For all calculations, the 6-31G(d) basis set[36] on all nonmetal atoms was used, while the LANL2DZ basis set with LANL2 effective core potential[37] was used for molybdenum. For calculating the solvent effects, geometry optimizations were performed on $[MoO(SCH_3)_4]^{1-/2-}$ using H_3CS^- to mimic the phenylthiolate ligands, and frequency calculations were conducted to ensure a minimum for the optimized geometry. The gas-phase optimized geometries were used for electronic structure calculation, and solvation calculations were conducted in respective solvents. The geometry reorganization energy in the Mo(IV) state was estimated as a difference between the energies for the molybdenum(IV) state as derived from the Mo(V) state and the optimized geometry. In the ligand calculations, the geometries were optimized using the B3LYP exchange functional with the 6-31G(d) basis set. The Mulliken[38] charges of all atoms of interest were calculated using standard procedures implemented in the Gaussian family software package; details are reported elsewhere.[39] Last, the percent contribution of atomic orbitals to their respective molecular orbitals was calculated by using the VMOdes program.[40]

Syntheses. Tris[(cyanoethoxy)methyl]aminomethane, [G1-CN] (1). Tris(hydroxymethyl) aminomethane (10 g, 82.5 mmol) was added to a mixture of aqueous KOH (500 mg, 9 mmol in 2.5 mL of water) and dioxane (10 mL) at room temperature. Next, acrylonitrile (17.6 mL, 268 mmol) was added to this mixture, and the mixture was vigorously stirred for 24 h. Excesses of acrylonitrile and dioxane were removed by evaporation to yield a yellow residue, which was dissolved in CH_2Cl_2 (100 mL). The organic layer was washed with water three times (total 300 mL) and dried over anhydrous Na_2SO_4. A pale yellow liquid was recovered in 80% yield (18.48 g) by evaporating the CH_2Cl_2 layer. ^{1}H NMR ($CDCl_3$): δ = 1.76 (br, 2H, NH_2); 2.63 (t, 6H, J = 6.0 Hz, CH_2); 3.45 (s, 6H, CH_2); 3.70 (t, 6H, J = 5.5 Hz, CH_2). ^{13}C NMR ($CDCl_3$): δ = 18.87, 65.82, 72.60 (CH_2); 56.16 ($C(CH_2)_3$); 118.09

(22) Bradbury, J. R.; Mackay, M. F.; Wedd, A. G. *Aust. J. Chem.* **1978**, *31*, 2423−2430.
(23) Stewart, J. J. P. *J. Comput.-Aided Mol. Des.* **1990**, *4*, 1−105.
(24) *HyperChem Pro. 6.03*; HyperCube, Inc.: Gainesville, FL, 2001.
(25) Becke, A. D. *J. Chem. Phys.* **1993**, *98*, 5648−5652.
(26) Lee, C.; Yang, W.; Parr, R. G. *Phys. Rev. B* **1988**, *37*, 785−789.
(27) Basis sets were obtained from the Extensible Computational Chemistry Environment Basis Set Database, Version 4/22/01, developed and distributed by the Molecular Science Computing Facility, Environmental and Molecular Sciences Laboratory which is part of the Pacific Northwest Laboratory, P.O. Box 999, Richland, WA 99352, and funded by the U.S. Department of Energy. The Pacific Northwest Laboratory is a multiprogram laboratory operated by Battelle Memorial Institute for the U.S. Department of Energy under Contract DE-AC06-76RLO 1830. Contact David Feller or Karen Schuchardt for further information.
(28) McLean, A. D.; Chandler, G. S. *J. Chem. Phys.* **1980**, *72*, 5639−5648. Krishnan, R.; Binkley, J. S.; Seeger, R.; Pople, J. A. *J. Chem. Phys.* **1980**, *72*, 650−654.
(29) Frisch, M. J.; Trucks, G. W.; Schlegel, H. B.; Scuseria, G. E.; Robb, M. A.; Cheeseman, J. R.; Zakrzewski, V. G.; Montgomery, J. A., Jr.; Stratmann, R. E.; Burant, J. C.; Dapprich, S.; Millam, J. M.; Daniels, A. D.; Kudin, K. N.; Strain, M. C.; Farkas, O.; Tomasi, J.; Barone, V.; Cossi, M.; Cammi, R.; Mennucci, B.; Pomelli, C.; Adamo, C.; Clifford, S.; Ochterski, J.; Petersson, G. A.; Ayala, P. Y.; Cui, Q.; Morokuma, K.; Malick, D. K.; Rabuck, A. D.; Raghavachari, K.; Foresman, J. B.; Cioslowski, J.; Ortiz, J. V.; Stefanov, B. B.; Liu, G.; Liashenko, A.; Piskorz, P.; Komaromi, I.; Gomperts, R.; Martin, R. L.; Fox, D. J.; Keith, T.; Al-Laham, M. A.; Peng, C. Y.; Nanayakkara, A.; Gonzalez, C.; Challacombe, M.; Gill, P. M. W.; Johnson, B. G.; Chen, W.; Wong, M. W.; Andres, J. L.; Head-Gordon, M.; Replogle, E. S.; Pople, J. A. *Gaussian 98*; Gaussian, Inc.: Pittsburgh, PA, 1998.
(30) Foresman, J. B.; Keith, T. A.; Wiberg, K. B.; Snoonian J.; Frisch, M. J. *J. Phys. Chem.* **1996**, *100*, 16098−16104.
(31) Wong, M. W.; Frisch, M. J.; Wiberg, K. B. *J. Am. Chem. Soc.* **1991**, *113*, 4776−4782. Wong, M. W.; Wiberg, K. B.; Frisch, M. J. *J. Am. Chem. Soc.* **1992**, *114*, 523−529.
(32) Perdew, J. P. *Phys. Rev. B* **1986**, *33*, 8822−8824.
(33) Kail, B.; Nemykin, V. N.; Davie, S. R.; Carrano, C. J.; Hammes, B.; Basu, P. *Inorg. Chem.* **2002**, *41*, 1481−1291.
(34) Nemykin, V. N.; Basu, P. *Inorg. Chem.* **2003**, *42*, 4046−4056.
(35) Thoomson, L. M.; Hall, M. B. *J. Am. Chem. Soc.* **2001**, *123*, 3995−4002.
(36) Ditchfield, R.; Hehre, W. J.; Pople, J. A. *J. Chem. Phys.* **1971**, *54*, 724−728.
(37) Hay, P. J.; Wadt, W. R. *J. Chem. Phys.* **1985**, *82*, 270−283.
(38) Mulliken, R. S. *J. Chem. Phys.* **1955**, *23*, 1833−1840, 1841−1846, 2338−2342, 2343−2346.
(39) Sengar, R. S.; Nemykin, V. N.; Basu, P. *New J. Chem.* **2003**, *27*, 1115−1123.
(40) Nemykin, V. N.; Basu, P. *VMOdes: Virtual Molecular Orbital description program for Gaussian, GAMESS, and HyperChem*, revision B 6.2, 2001.

(CN). ESI$^+$-MS (CH_3CN): *m/z* 281.1 $[M + H]^+$ ($M = C_{13}H_{20}N_4O_3$, 280.2); 303.1 $[M + Na]^+$. IR (NaCl): 3371 cm^{-1}, 3350 cm^{-1} (ν_{NH}); 2916 cm^{-1}, 2877 cm^{-1} (ν_{CH}); 2251 cm^{-1} ($\nu_{C\equiv N}$).

Tris[((ethoxycarbonyl)ethoxy)methyl]aminomethane, [G1-Ester] (2). *p*-Toluenesulfonic acid monohydrate (21.96 g, 0.12 mol) and absolute ethanol (6.77 mL, 0.12 mol) were added to **1** (10.79 gm, 0.04 mol), and refluxed with stirring for 6 h. During the reaction, the ammonium salt of *p*-toluenesulfonic acid formed. Toluene (10 mL) was added into the reaction for smooth stirring, and the precipitate was filtered and washed with toluene. After it was washed, the filtrate was dissolved in CH_2Cl_2 and washed with saturated $NaHCO_3$ solution several times. The organic layer was removed and dried over anhydrous $MgSO_4$ and evaporated to give a yellow liquid at a 50% (8.42 gm) yield. ^{1}H NMR ($CDCl_3$): $\delta =$ 1.27 (t, 9H, $J = 6.6$ Hz, CH_3); 1.74 (br, 2H, NH_2); 2.55 (t, 6H, $J = 6.4$ Hz, CH_2); 3.32 (s, 6H, CH_2); 3.69 (t, 6H, $J = 6.1$ Hz, CH_2); 4.15 (qt, 6H, $J = 6.8$ Hz, CH_2). ^{13}C NMR ($CDCl_3$): $\delta = 14.06$ (CH_3); 34.97, 60.22, 66.74, 72.66 (CH_2); 55.86 ($C(CH_2)_3$); 171.36 (CO_2Et). ESI$^+$-MS (CH_3CN): *m/z* 422.2 $[M + H]^+$ ($M = C_{19}H_{35}NO_9$, 421). IR (NaCl): 3379 cm^{-1}(ν_{NH});, 2982 cm^{-1}, 2873 cm^{-1} (ν_{CH}); 1736 cm^{-1} ($\nu_{C=O}$).

4,4′-Dithiobenzoic acid (3). A saturated solution of I_2 in 95% ethanol was slowly added to an ethanol solution (100 mL) of 4-mercaptobenzoic acid (1.5 g, 9.74 mmol). As the reaction progressed, the brown color of iodine disappeared with a precipitation. The addition of iodine solution was continued until a light yellow color of the reaction mixture persisted. The off-white precipitate was collected and washed with ethanol, followed by drying under reduced pressure at 50 °C to remove any adsorbed iodine to obtain the final product at a 98% yield (1.47 g). ^{1}H NMR (DMSO-d_6): $\delta = 7.63$ (d, 4H, $J = 8.2$ Hz, arom CH); 7.93 (d, 4H, $J = 8.5$ Hz, arom CH). ^{13}C NMR (DMSO-d_6): $\delta = 126.12$, 129.70, 130.23, 140.74 (arom C); 166.58 (CO_2H). ESI$^-$-MS (CH_3OH): *m/z* 305.0 $[M - H]^-$ ($M = C_{14}H_{10}O_4S_2$, 306). IR (KBr): 3444 cm^{-1} (ν_{OH}); 2981 cm^{-1} (ν_{CH}); 1686 cm^{-1} (ν_{CO}); 759 cm^{-1} (ν_{CH} bend).

Disulfide of G_0-Amide (4a). This compound has been synthesized according to the literature procedure.[39] Yield 65%. ^{1}H NMR (DMSO-d_6): $\delta = 2.74$ (d, 6H, $J = 4.5$ Hz, CH_3); 7.60 (d, 4H, $J =$ 8.5 Hz, arom CH); 7.82 (d, 4H, $J = 8.5$ Hz, arom CH); 8.46 (m, 2H, NH). ^{13}C NMR (DMSO-d_6): $\delta = 24.08$, 26.15 (CH_3); 126.28, 128.14, 133.54, 138.58 (arom C); 165.72 (CONH). ESI$^+$-MS (CH_3OH): *m/z*: 333.0 $[M + H]^+$ ($M = C_{16}H_{16}N_2O_2S_2$, 332). ESI$^-$-MS ($CH_3OH$): *m/z* 330.9 $[M - H]^-$ ($M = C_{16}H_{16}N_2O_2S_2$, 332). IR (KBr): 3321.5 cm^{-1} (ν_{NH}); 1637 cm^{-1} (ν_{CO}); 1593 cm^{-1} (ν_{CONH}).

Disulfide of [G_1-CN]-Amide (4b). The acid chloride of **3**[39] (1.5 g, 4.9 mmol) was reacted with the dendron, **1** (3.5 g, 12.5 mmol), in CH_2Cl_2 (20 mL) in the presence of triethylamine (2.62 mL, 18.75 mmol) in CH_2Cl_2 (15 mL) as described for **4a**. After 24 h of stirring, the reaction was quenched by adding 10 mL of water, and the organic layer was withdrawn and washed with 15 mL of (1 N) HCl solution, followed by 15 mL of 10% $NaHCO_3$ solution, and drying over anhydrous Na_2SO_4. The organic layer was collected by filtration and was evaporated to dryness to yield a light yellow oily compound. Next, the oil was purified by adsorption chromatography on silica gel with a 1:3 mixture of MeCN and toluene. Yield is 85% (3.45 g).^{1}H NMR ($CDCl_3$): $\delta = 2.61$ (t, 12H, $J =$ 5.9 Hz, CH_2); 3.72 (t, 12H, $J = 6.0$ Hz, CH_2); 3.95 (s, 12H, CH_2); 6.43 (s, 2H, NH); 7.52 (d, 4H, $J = 8.3$ Hz, arom CH); 7.71 (d, 4H, $J = 8.6$ Hz, arom CH). ^{13}C NMR ($CDCl_3$): $\delta = 18.81$, 65.79, 69.15 (CH_2); 60.01 ($C(CH_2)_3$); 117.99 (CN); 126.67, 127.82, 133.51, 140.50 (arom C); 166.76 (CONH). ESI$^+$-MS (CH_3CN): *m/z*: 831.2 $[M + H]^+$ ($M = C_{40}H_{46}N_8O_8S_2$, 830.3); 853.2 $[M + Na]^+$. IR (NaCl): 3416 cm^{-1} (ν_{NH}); 2916 cm^{-1}, 2887 cm^{-1} (ν_{NH}); 2252 cm^{-1} ($\nu_{C\equiv N}$), 1733 cm^{-1} and 1661 cm^{-1} (ν_{CONH}).

Disulfide of [G_1-Ester]-amide (4c). This compound was synthesized following the procedure outlined for **4b** using **3** (1.0 gm, 3.27 mmol), **2** (3.44 g, 8.17 mmol), and triethylamine (1.7 mL 12.3 mmol) in CH_2Cl_2 (25 mL). The crude product was purified by adsorption chromatography on silica gel using a 1:2 mixture of MeCN and toluene to yield 89% (3.24 g).^{1}H NMR ($CDCl_3$): $\delta =$ 1.22 (t, 18H, $J = 7.0$ Hz, CH_3), 2.53 (t, 12H, $J = 6.3$ Hz, CH_2), 3.71 (t, 12H, $J = 6.2$ Hz, CH_2), 3.82 (s, 12H, CH_2), 4.10 (qt, 12H, $J = 7.0$ Hz, CH_2), 6.55 (s, 2H, NH), 7.50 (d, 4H, $J = 8.5$ Hz, arom CH), 7.73 (d, 4H, $J = 8.5$ Hz, arom CH). ^{13}C NMR ($CDCl_3$): $\delta =$ 13.47 (CH_3); 34.23, 59.55, 66.10, 68.44 (CH_2); 50.69 ($C(CH_2)_3$); 125.63, 127.29, 133.44, 139.22 (arom C); 165.59 (CONH), 170.64 (CO_2Et). FAB$^+$-MS: *m/z*: 1113.0 $[M + H]^+$ ($M = C_{52}H_{76}N_2O_{20}S_2$, 1112). 1023.0 $[M - 2OEt]^+$ ($M = C_{52}H_{76}N_2O_{20}S_2$, 1112). ESI$^+$-MS ($CH_3CN$): *m/z*: 1113.3 $[M + H]^+$; 1135.2 $[M + Na]^+$. IR (NaCl): 3418 cm^{-1} (ν_{NH}); 2982 cm^{-1}, 2877 cm^{-1} (ν_{CH}); 1734 cm^{-1} (ν_{CO}); 1666 cm^{-1} (ν_{CONH}).

Thiol of [G_1-CN]-Amide (5b). Compound **4b** (1.65 g, 1.99 mmol) was dissolved in a mixture of dry EtOH/THF (15 mL/15 mL), and $NaBH_4$ (0.3 g, 7.96 mmol) was added in small portions at 0 °C under Ar atmosphere. After the complete addition of the $NaBH_4$, the temperature was raised to room temperature, and the reaction mixture was allowed to stir for 4 h. After removing the solvents under reduced pressure, the resulting yellow solid was dissolved in distilled water (10 mL), and 0.5 N HCl was added to acidify the solution to pH $\sim$ 4. A yellowish oily material separated out from the solution, which was extracted with EtOAc (60 mL) and dried over anhydrous $MgSO_4$. Evaporation of the EtOAc solution yielded a yellow liquid, which was purified by adsorption chromatography on silica gel using a 1:3 mixture of MeCN and toluene to yield 90% (1.49 g) of final product. ^{1}H NMR ($CDCl_3$): $\delta = 2.62$ (t, 6H, $J = 6.1$ Hz, CH_2); 3.72 (t, 6H, $J = 5.7$ Hz, CH_2); 3.96 (s, 6H, CH_2); 6.46 (s, 1H, NH); 7.23 (d, 2H, $J = 7.9$ Hz, arom CH); 7.65 (d, 2H, $J = 8.2$ Hz, arom CH). ^{13}C NMR ($CDCl_3$): $\delta = 18.32$, 65.32, 68.66 (CH_2); 59.52 ($C(CH_2)_3$); 117.72 (CN); 127.33, 127.93, 131.16, 136.03 (arom C); 166.51 (CONH). ESI$^+$-MS (CH_3CN): *m/z*: 417.2 $[M + H]^+$ ($M = C_{20}H_{24}N_4O_4S$, 416.2); 439.2 $[M + Na]^+$. ESI$^-$-MS (CH_3CN): *m/z*: 415.2 $[M - H]^-$. IR (NaCl): 3417 cm^{-1} (ν_{NH}); 2937 cm^{-1}, 2883 cm^{-1} (m, ν_{CH}); 2559 cm^{-1} (ν_{SH}); 2252 cm^{-1} ($\nu_{C\equiv N}$); 1734 cm^{-1} ($\nu_{C=O}$); 1659 cm^{-1} (ν_{CONH}).

Thiol of [G_1-Ester]-amide (5c). This compound was synthesized as **5b** using **4c** (1.0 g, 0.9 mmol) and $NaBH_4$ (0.14 g, 3.6 mmol) in a mixture of dry EtOH/THF (10 mL/10 mL). The purified compound was isolated in 96% yield (0.95 mg) as a yellow liquid. ^{1}H NMR ($CDCl_3$): $\delta = 1.24$ (t, 9H, $J = 7.0$ Hz, CH_3), 2.55 (t, 6H, $J = 6.4$ Hz, CH_2), 3.73 (t, 6H, $J = 6.4$ Hz, CH_2), 3.82 (s, 6H, CH_2), 4.12 (qt, 6H, $J = 6.8$ Hz, CH_2), 6.53 (s, 1H, NH), 7.26 (d, 2H, $J = 5.7$ Hz, arom CH), 7.64 (d, 2H, $J = 7.8$ Hz, arom CH). ^{13}C NMR ($CDCl_3$): $\delta = 13.74$ (CH_3); 34.54, 59.87, 66.34, 68.76 (CH_2); 59.61 ($C(CH_2)_3$); 127.39, 127.80, 131.70, 135.49 (arom C); 166.19 (CONH); 170.99 (CO_2Et). ESI$^+$-MS (CH_3CN): *m/z*: 580.2 $[M + Na]^+$ ($M = C_{26}H_{39}NO_{10}S$, 557.2). ESI$^-$-MS (CH_3CN): *m/z*: 556.2 $[M - H]^-$. IR (NaCl): 3421 cm^{-1} (ν_{NH}); 2981 cm^{-1}, 2877 cm^{-1} (m, ν_{CH}), 2559 cm^{-1} (ν_{SH}), 1735 cm^{-1} ($\nu_{C=O}$), 1664 cm^{-1} (ν_{CONH}).

$(PPh_4)[MoO(SPh)_4]$ (6). This compound was synthesized according to the published procedure[41] by reacting $MoOCl_3(THF)_2$

(41) Boyd, I. W.; Dance, I. G.; Murray, K. S.; Wedd, A. G. *Aust. J. Chem.* **1978**, *31*, 279−284.

Scheme 1

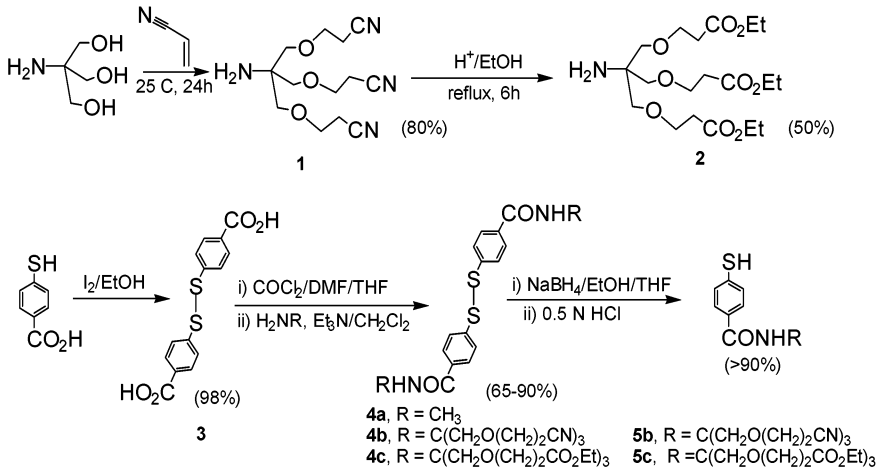

with thiophenol in a Et_3N/MeCN solution. UV−vis spectra [λ_{max}, nm (ϵ, M^{-1} cm^{-1}), MeCN]: 602 (6960). EPR g parameter: ($g_{||}$, 2.017); ($g_{\perp}$, 1.979); (g_{av}, 1.992). IR (KBr): 943 cm^{-1} ($\nu_{Mo=O}$). ESI$^-$-MS (CH_3CN): m/z 550.7 [M − PPh_4]$^-$ ($M = C_{24}H_{20}OS_4Mo$, 550).

(PPh_4)[MoO(p-$SC_6H_4CONHCH_3$)] (7a). A mixture of **6** (40 mg, 0.45 mmol) and **4a** (120 mg, 0.36 mmol) was stirred in THF (12 mL) at room temperature for 48 h, resulting in a dark precipitate. The precipitate was filtered from the reaction mixture and washed with 30 mL of 1,2-dimethoxyethane (DME), and cold THF (30 mL). Finally, the residue was recrystallized from a MeCN/DME mixture. Yield 40% (20 mg). UV−vis [λ_{max}, nm (ϵ, M^{-1} cm^{-1}), MeCN]: 599 (4800), 330 (20906), 265 (75262), 230 (96168). EPR g parameter: ($g_{||}$, 2.018); ($g_{\perp}$, 1.988); (g_{av}, 1.998). IR (KBr): 3342 cm^{-1} (ν_{NH}), 3048 cm^{-1}, 2941 cm^{-1} (ν_{CH}), 1659 cm^{-1} ($\nu_{C=O}$), 1588 cm^{-1} (ν_{CONH}), 943 cm^{-1} ($\nu_{Mo=O}$). ESI$^-$-MS (CH_3CN): m/z 778 [M − PPh_4]$^-$ ($M = C_{32}H_{32}N_4O_5S_4Mo$, 778).

(PPh_4)[MoO(p-SC_6H_4-G1CN)$_4$] (7b). Cold dry degassed THF (10 mL) was added to a precooled Schlenk flask containing $MoCl_5$ (55 mg, 0.2 mmol) at −78 °C. After the complete addition, the reaction mixture was slowly warmed to room temperature, and during this period, the initial brown-red color of the solution changed to green. After 10 min, a solution containing **5a** (500 mg, 1.2 mmol) and triethylamine (0.16 mL, 1.2 mmol) in dry degassed THF (10 mL) was added over a period of 5 min. Upon addition, the color of the reaction mixture turned blue and was stirred for an additional 10 min and filtered. To the filtrate a solution of PPh_4Cl (110 mg, 0.3 mmol) in 10 mL of methanol was added, followed by evaporation under reduced pressure. The resultant residue was redissolved in THF and purified by size exclusion chromatography using BioBeads SX-3 using THF as an eluent. Yield 28% (120 mg). UV−vis [λ_{max}, nm (ϵ, M^{-1} cm^{-1}), MeCN]: 601 (5390), 412 (13766), 335 (45894), 267 (133918), 225 (152485). EPR g parameter: ($g_{||}$, 2.022); ($g_{\perp}$, 1.984); (g_{av}, 1.997). IR (NaCl): 3426 cm^{-1} (m, ν_{NH}), 3066 cm^{-1}, 2955 cm^{-1} (ν_{CH}), 2249 cm^{-1} ($\nu_{C\equiv N}$), 1665 cm^{-1} ($\nu_{C=O}$), 1588 cm^{-1} (ν_{CONH}), 948 cm^{-1} ($\nu_{Mo=O}$). ESI$^-$-MS (CH_3CN): m/z: 1774 [M − PPh_4]$^-$ ($M = C_{80}H_{92}N_{16}O_{17}S_4$-Mo, 1774).

(PPh_4)[MoO(p-SC_6H_4-G1Ester)$_4$] (7c). This compound was synthesized following the procedure described for **7b**. Yield 31%. UV−vis [λ_{max}, nm (ϵ, M^{-1} cm^{-1}), MeCN]: 602 (5840), 410 (9259), 336 (33777), 267 (74800), 225 (118518). EPR g parameter: ($g_{||}$, 2.020); ($g_{\perp}$, 1.983); (g_{av}, 1.995). IR (NaCl): 3426 cm^{-1} (m, ν_{NH}), 2981 cm^{-1}, 2960 cm^{-1} (ν_{CH}), 1660 cm^{-1}, 1731 cm^{-1} ($\nu_{C=O}$), 1588 cm^{-1} (ν_{CONH}), 944 cm^{-1} ($\nu_{Mo=O}$). ESI$^-$-MS (CH_3CN): m/z 2339 [M − PPh_4]$^-$ ($M = C_{104}H_{152}N_4O_{41}S_4Mo$, 2339).

Results

1. Synthesis of Ligands and Metal Complexes. The synthetic methodology of dendritic units (dendrons) closely followed those reported in the literature.[42] The synthetic approach is shown in Scheme 1. The polyether dendritic nitrile (**1**) was synthesized by reacting tris(hydroxymethyl) aminomethane (tris) and acrylonitrile in dioxane, which was then purified by a series of solvent extractions using CH_2Cl_2 and water. The ester-terminated dendron, **2**, was synthesized by hydrolyzing the nitrile group with *p*-toluenesulfonic acid in ethanol and toluene. Although Newkome and co-workers originally used hydrochloric acid to hydrolyze the nitrile groups,[43] in our hands *p*-toluenesulfonic acid afforded cleaner reactions. The reaction was probed by IR spectroscopy monitoring the disappearance of the nitrile stretching. Both dendrons were synthesized in spectroscopically pure forms in very good yields. To synthesize the dendritic ligands, the amine terminals were linked with the carboxyl groups of derivatized benzene thiols. The thiol group was first protected through oxidation to the corresponding disulfide using iodine as an oxidant. The disulfide (**3**) precipitated out of the solution and was collected by filtration and dried under reduced pressure. In some cases, an excess of adsorbed iodine complicates subsequent reactions, and required removal by sublimation.

The carboxyl groups of **3** were reacted with oxalyl chloride in dry THF and a trace amount of DMF; the solvent was evaporated to dryness affording the corresponding acid chloride that was reacted in CH_2Cl_2 directly with the dendrons in the presence of triethylamine. The coupling reactions were conducted overnight and quenched with water. The amide compounds were extracted with CH_2Cl_2 and chromatographed on silica gel. With the exception of **4a**, the target disulfide amide compounds were eluted as yellow bands using a 1:3 mixture of MeCN−toluene as eluent. All disulfides were synthesized in very good to excellent yields (82−98%). The G_0-disulfide, (p-$SC_6H_4CONHCH_3)_2$ (**4a**), was isolated as a white solid, whereas first generation nitrile

(42) Newkome, G. R.; Lin, X. *Macromolecules* **1991**, *24*, 1443−1444.
(43) Newkome, G. R.; Lin, X.; Young, J. K. *Synth. Lett*. **1992**, 53−54.

Scheme 2

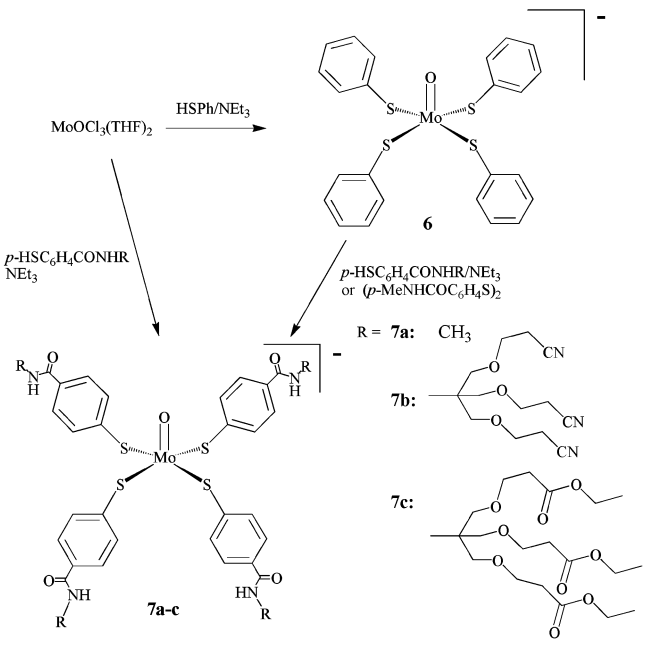

terminated [*p*-$SC_6H_4CONHC(CH_2O(CH_2)_2CN)_3]_2$ (**4b**) and ester terminated [*p*-$SC_6H_4CONHC(CH_2O(CH_2)_2CO_2Et)_3]_2$ (**4c**) disulfides were isolated as yellow liquids. The disulfides (**4b** and **4c**) were reduced to dendritic thiols [*p*-HSC_6H_4-$CONHC(CH_2O(CH_2)_2CN)_3]$ (**5b**) and [*p*-HSC_6H_4CONHC-$(CH_2O(CH_2)_2CO_2Et)_3]$ (**5c**) with sodium borohydride in a 1:1 mixture of ethanol and THF. The corresponding thiols were isolated as light yellow oils in excellent yields (90−95%). The thiols were found to be moderately air sensitive, especially in solution.

In general, three distinct routes have been described for synthesizing the oxo−molybdenum(V) tetrathiolato complexes. The first method involves a halogen substitution reaction from either $[Mo^VOCl_5]^{2-}$ or $MoOCl_3(THF)_2$ with thiolato ligands in the presence of a base, usually triethylamine. The second method also involves exchange of thiophenolato ligands with substituted aryl thiols. This method has been utilized to synthesize a wide variety of complexes including alkanethiols. Finally, the tetrathiolate oxo−molybdenum(V) complexes have been synthesized by exchanging the thiophenolato groups in $[Mo^VO(SPh)_4]^-$ with aryl disulfides via redox-coupled ligand exchange reaction.[44] Such redox-coupled ligand exchange reactions have been described for synthesizing other metal−sulfur cores such as iron−sulfur clusters.[45] The redox coupled ligand exchange reactions have been attempted for the synthesis of **7a**, **7b**, and **7c**. However, only complex **7a** was successfully synthesized by exchanging the thiophenolato groups of $[PPh_4]$-$[Mo^VO(SPh)_4]$ (**6**) using disulfide **4a** (Scheme 2). The ESI MS of the crude product suggests a mixture of the general formula $[Mo^V(SPh)_n(p\text{-}SC_6H_4CONHCH_3)_{4-n}]^-$ even in the presence of a large excess (7 times) of the disulfide, **4a**. In contrast, the thiophenolato complexes of the *o*-substituted ligands afford pure materials with only a slight excess of the ligand.[44] One possible reason for such a difference is that the conformation of the *o*-substituted ligand geometry allows for hydrogen bond formation between the NH proton and the thiolato sulfur, which significantly alters the redox potential of the ligands. Fortunately, complex **7a** can be separated from the reaction mixture by recrystallization from MeCN/DME solutions. When the same methodology was applied for the preparation of **7b** and **7c**, an incomplete exchange of the thiophenolato group was observed, presumably due to the steric constraint. Instead of using the disulfides (**4b** and **4c**), complexes **7b** and **7c** were synthesized by using excess (∼6 times) of the thiols (**5b** and **5c**), followed by repeated cycles of size exclusion chromatography from the evaporated residues of the reaction mixture. In each case, the target compound could be eluted with THF as the second dark blue band, and the evaporation of the organic solvent resulted in a pure complex. Because this procedure requires substantial time to purify the target compounds, we exploited the alternative halogen exchange reaction from $MoOCl_3$-$(THF)_2$ with the dendritic thiols. Using this strategy, we have synthezised $[Mo^VO(SAr)_4]^-$ cores without the complication of incomplete thiol substitution reaction. The dendritic molecules (**7b** and **7c**) were finally purified by size exclusion chromatography. Although the yields of the complexes were lower as compared to those of the thiol exchange reactions, the purity was higher, and the purification procedure was more convenient. All of the oxo−molybdenum(V) complexes were synthesized as tetraphenyl phosphonium salts. Complexes **6** and **7a** were isolated in solid form whereas compounds **7b** and **7c** were isolated as gummy materials. All molybdenum compounds reported here are soluble in common organic solvents such as MeCN, DMF, CH_2Cl_2, and CH_3OH, although the molybdenum complexes of dendritic ligands are unstable in chlorinated solvents or protic solvents and are extremely sensitive to air.

2. Spectral Characterization of Molecules. All dendrons and ligands were characterized by ESI-MS, ^1H and ^{13}C NMR, and IR spectroscopies. For disulfides, the chemical shifts of the aromatic protons were slightly different from those of the thiols, serving as good indicators of the purity of the materials. The ^{13}C NMR chemical shift is known to correlate with the Hammett constants, and we have used the ^{13}C NMR chemical shifts to parametrize the Hammett constants for the dendritic molecules.[39] In the positive mode ESI-MS, often the ions were found to be associated with a sodium ion, which is a common phenomenon when bulky or biological molecules are investigated. The IR spectra of the nitrile-terminated dendrons and ligands exhibit a strong absorption ∼2250 cm^{-1} that served as a diagnostic feature for the presence of a −CN group, which was used to probe the progress of reactions involving −CN group.

All oxo−molybdenum(V) compounds (**6**, **7a**−**c**) have been characterized by mass spectrometry, IR spectroscopy, EPR and electronic spectroscopy. The molecular mass for compounds **6** and **7a**−**c** has been determined by negative ion ESI-MS from their MeCN solutions (Figure 2). The mass-

(44) Ueyama, N.; Okamura, T.; Nakamura, A. *J. Am. Chem. Soc*. **1992**, *114*, 8129−8137.
(45) Que, L. J.; Bobrik, M. A.; Ibers, J. A.; Holm, R. H. *J. Am. Chem. Soc*. **1974**, *96*, 4168−4178.

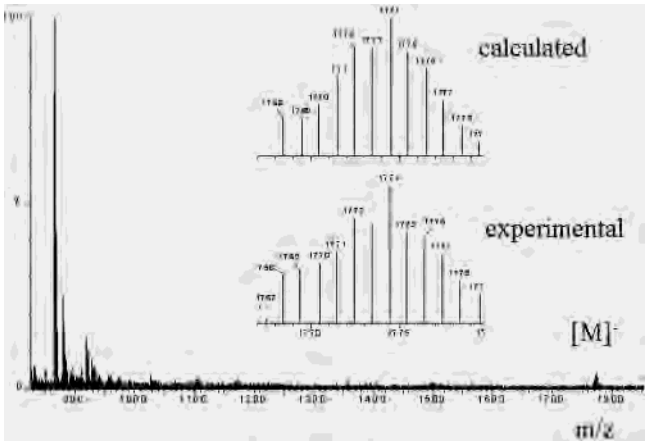

Figure 2. ESI-MS of **7c** and the theoretical distribution of the anion.

to-charge ratio and the isotope distribution pattern agreed well with the theoretical value for tetrasubstituted dendritic complexes. Furthermore, mass spectrometry confirmed that there is no branching defect in the ligand architecture. Interestingly, both the fast atom bombardment mass spectrometry (FABMS) and the matrix assisted laser desorption ionization (MALDI) mass spectrometry were unsuccessful in providing molecular ion peaks. Also at higher temperatures, ESI-MS exhibited spectra with polymeric patterns, which are currently under investigation. In addition to C≡N, C═O, and N−H vibrations, the Mo═O^t vibration has also been probed by infrared spectroscopy. Infrared spectra of gummy samples were measured on a salt plate, while those for the solid samples were recorded in KBr pellets. The Mo═O^t vibration has been observed at the same frequency as those of other tetrathiophenolato complexes.[46] Practically no variation was observed in the Mo═O^t stretching frequency (943−948 cm^{-1}) within the complexes (**6**, **7a**−**c**) reported here, suggesting that the Mo═O^t bond strength in these molecules is very similar. The oxo−molybdenum(V) complexes **6** and **7a**−**c** exhibit an intense low energy absorption band at ∼600 nm ($\epsilon \sim 6000$ M^{-1} cm^{-1}) (Figure 3) with the largest variation in the band maxima being less than 5 nm. This is a very intriguing result, which is in contrast to the peripherally substituted thiophenolato or structurally rigid hydrotris(pyrazolyl)borate complexes that show a linear dependence of the low energy charge transfer transition as a function of substituents.[46,47] In our molecules, the maximum of the broad charge transfer band, however, is invariant with the Hammett constant of the ligand. In order to understand the solvochromic nature of this low energy band, we have recorded optical spectra of [Mo^{V}O(SPh)$_4$]$^-$ in CH_2Cl_2, MeCN, propylene carbonate (PC), DMSO, and DMF. In all cases, the band maxima appeared at the same position, and the peak width also remained similar indicating no appreciable solvochromic effect (Figure S1). It is instructive to point out that this broad band is a composite of several overlapping transitions involving the low lying sulfur based orbitals and the d-manifolds. We have investigated the nature of this transition using magnetic circular dichroism (MCD) spectroscopy;[48] general features are in agreement with those reported for [Mo^{V}O(SPh)$_4$]$^-$.[49]

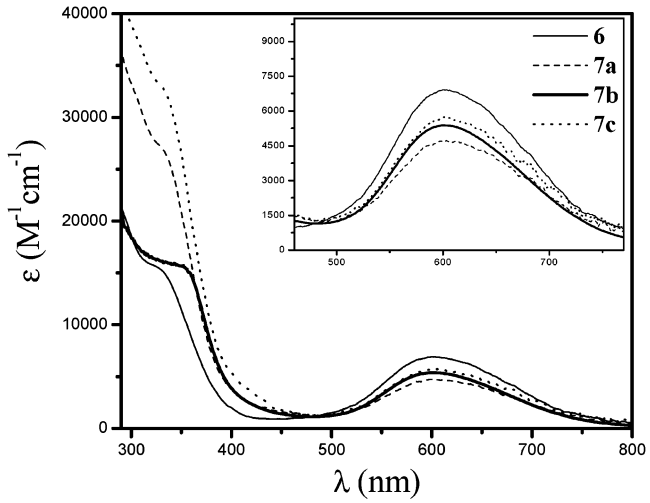

Figure 3. Room temperature electronic spectra of Mo complexes **6** and **7a**−**c** in MeCN solutions.

This low energy transition is a sensitive reporter of distortions at the metal center. For example, in [MoO(S$_2$bph)$_2$] (where S$_2$bph = bis-thiophenol, a rigid ligand), this transition shifted by 30 nm.[50] It is important to note that the position of the low-energy transition is not affected by the architecture of ligands, suggesting the orientation of the S π orbitals with respect to the Mo d_{xy} orbital is similar. The orientation not only modulates the energy of the transition but also the oscillator strengths. A similar orbital control is now established for other metal centers such as in the Cu−cysteine in blue copper centers[51] and in heme.[52] The near invariant band position as well as similar oscillator strength strongly argues that the addition of bulkier dendritic ligands does not alter the orientation of the π orbitals with respect to the metal d_{xy} orbital. Thus, relative orientation and position of the sulfurs are almost similar to each other.

The oxo-molybdenum(V) complexes (**7a**−**c**) are paramagnetic with an $S = {}^1/_2$ (d^1) ground state and are amenable to EPR spectroscopy (Figure 4). The molybdenum complexes exhibit axial EPR spectra similar to those observed by Hanson et al. for [Mo^{V}O(SPh)$_4$]$^-$.[53] In addition, the characteristic molybdenum hyperfine structures, due to the presence of naturally abundant $I = {}^5/_2$ isotopes (25% of total contribution), have also been observed. No significant variation in the g-values has been observed in these complexes, indicating that the integrity of the square

(46) Ellis, S. R.; Collision, D.; Garner, C. D. *J. Chem. Soc., Dalton Trans.* **1989**, 413−417.
(47) Chang, C. S. J.; Collison, D.; Mabbs, F. E.; Enemark, J. H. *Inorg. Chem.* **1990**, *29*, 2261−2267.
(48) McNaughton, R. L.; Nemykin, V. N.; Mondal, S.; Basu, P.; Kirk, M. L. Manuscript in preparation.
(49) (a) McMaster, J.; Carducci, M. D.; Yang, Y. S.; Solomon, E. I.; Enemark, J. H. *Inorg. Chem.* **2001**, *40*, 687−702. (b) McNaughton, R. L.; Tipton, A. A.; Rubie, N. D.; Conry, R. R.; Kirk, M. L. *Inorg. Chem.* **2000**, *39*, 5697−5706.
(50) Conry, R. R.; Tipton, A. A. *JBIC, J. Biol. Inorg. Chem.* **2001**, *6*, 359−366.
(51) Holm, R. H.; Kennepohl, P.; Solomon, E. I. *Chem. Rev.* **1996**, *96*, 2239−2314.
(52) Walker, F. A. *Coord. Chem. Rev.* **1999**, *185*−*186*, 471−534.
(53) Hanson, G. R.; Wilson, G. L.; Bailey, T. D.; Pilbrow, J. R.; Wedd, A. G. *J. Am. Chem. Soc.* **1987**, *109*, 2609−2616.

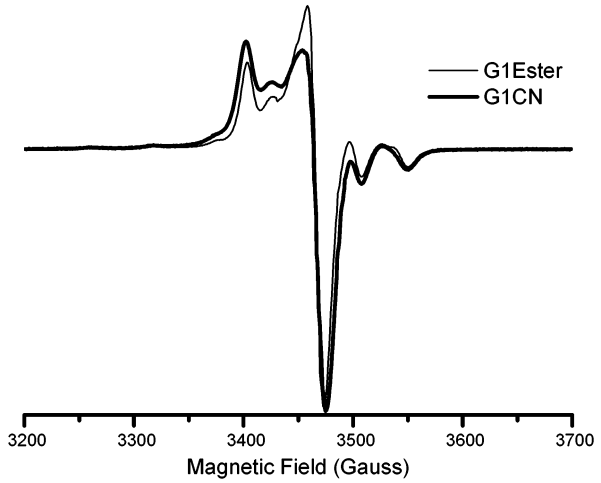

Figure 4. X-band CW-EPR spectra of frozen solutions of **7b** (thick line labeled as G1CN) and **7c** (thin line labeled as G1-ester) at 20K.

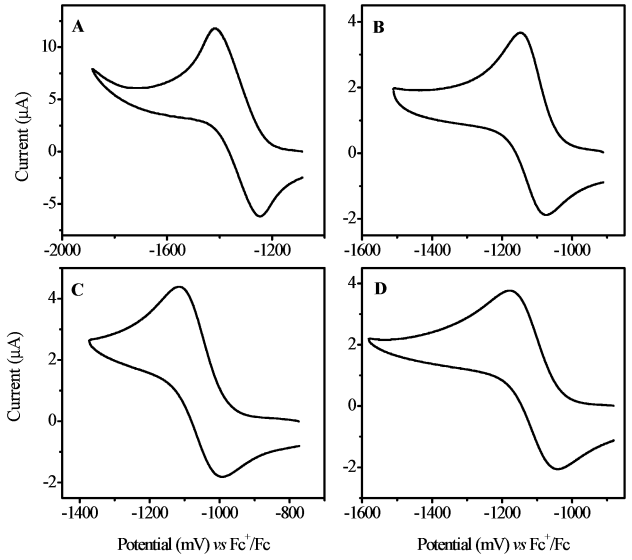

Figure 5. Cyclic voltammograms of **6** (A), **7a** (B), **7b** (C), and **7c** (D) in MeCN solution (scan rate 100 mV/s).

pyramidal $[Mo^{V}OS_4]^-$ core (C_{4v} local symmetry) is retained. Thus, again, the EPR data in agreement with the UV−vis spectra of complexes **6** and **7a**−**c** suggest that the addition of bulky and symmetric dendritic architecture does not impose any appreciable distortion at the metal center in the frozen solution.

3. Electrochemical Behavior of the Molybdenum Complexes. The redox chemistry of the molybdenum complexes was investigated using cyclic voltammetry in MeCN, DMF, and propylene carbonate. Figure 5 shows cyclic voltammograms recorded in MeCN, and all potentials are listed in Table 1. The solvents were chosen to span a wide range of dielectric constant and stability of the molybdenum complexes. In each case, the half wave potential was obtained by digitally simulating cyclic voltammograms. An EC mechanism (electron transfer followed by a chemical transformation) was used to simulate the cyclic voltammograms (a detailed study of digital simulation will be communicated elsewhere). The potentials are internally calibrated and expressed with respect to the ferrocenium/ferrocene couple.

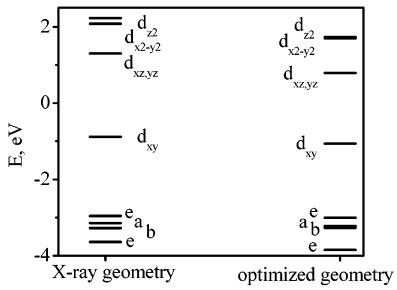

Figure 6. Calculated molecular orbital diagrams for the optimized and the X-ray derived structure for $[MoO(SPh)_4]^-$.

Table 1. Mo(V/IV) Reduction Potentials $E_{1/2}$, mV (ΔE_p, mV), at 25 C[a]

solvent	6	7a	7b	7c
MeCN	−1321 (122)	−1171 (70)	−1097 (122)	−1117 (137)
DMF	−1383 (89)	−1213 (68)	−1251 (167)	−1247 (335)
PC	−1324 (114)	−1084 (69)	−1052 (138)	−1099 (269)

[a] Potentials vs Fc^+/Fc.

The anion displays a well-defined couple due to the reduction of Mo(V) to Mo(IV), similar to those observed by Bradbury et al.,[54] but no oxidative response could be observed within the solvent window. In all compounds (**6**, **7a**−**c**), the reversibility of this reduction was supported by different scan rate experiments, which show a linear relationship between square root of the scan rate and current observed (Figure S2). In a separate experiment, the influence of the electrolyte concentration on the reduction potentials of complex **6** was investigated. It has been found that, in the 0.1−0.4 M electrolyte concentration range, the reduction potential is practically constant (the maximum deviation found to be 16 mV). With increasing steric bulk at the ligand, the irreversibility also increased as demonstrated by the peak-to-peak separation. For all compounds, the peak−peak separation was larger in propylene carbonate and in DMF as compared to acetonitrile.

4. Electronic Structure Calculations. The electronic structures of $[MoO(SPh)_4]^-$ and $[MoO(p\text{-}SC_6H_4CONHCH_3)_4]^-$ complexes were calculated both in the restricted and unrestricted formalism using the DFT method with the B3LYP EC functional. Calculations were conducted for both X-ray idealized and optimized geometries in order to understand the effect of the geometry optimization on the electronic structure. The results of these calculations are presented in Figure 6 and in Tables 2, 3, and S1. The average bond distances and angles of the optimized geometry deviate from the X-ray crystallographically determined geometry by 0.07 Å and 0.93−1.22°, for the most important distances and angles, respectively (Table 2). In the optimized structures, the terminal oxo bonds are found to be longer than those in the X-ray structures. Such elongation stabilizes the orbitals aligned along the Mo═O vector; thus, the energy of difference between the Mo d_{z^2} and Mo $d_{x^2-y^2}$ orbitals is reduced. Calculations based on the X-ray geometry show that the difference in energy between the d_{z^2} and the $d_{x^2-y^2}$

(54) Bradbury, J. R.; Masters, A. F.; McDonell, A. C.; Brunette, A. A.; Bond, A. M.; Wedd, A. G. *J. Am. Chem. Soc.* **1981**, *103*, 1959−1964.

Table 2. Selected Geometric Parameters $[MoO(SAr)_4]^-$

		optimized geometry[a]	
	exptl geometry[22] $[MoO(SPh)_4]^-$	$[MoO(SPh)_4]^-$	$[MoO(p\text{-}SC_6H_4CONHMe)_4]^-$
Mo═O	1.67	1.72	1.72
Mo−S	2.40	2.49	2.49
S−C	1.76	1.84	1.84
O−Mo−S	109.86	109.46	109.74
Mo−S−C	109.82	109.33	108.97
O−Mo−S−C	58.81	56.04	56.99
av deviation[b]		0.07/1.22	0.07/0.93

[a] Optimized using LANL2DZ basis set for all the atoms. [b] rmsd for distances/angles compared to the crystallographic geometry. In the case of $[MoO(p\text{-}SC_6H_4CONHMe)_4]^-$, the crystal structure of $[MoO(SPh)_4]^-$ was used.

orbitals is about 0.15 eV for $[MoO(SPh)_4]^-$, while it is only 0.03 eV for the geometry-optimized structure. Because the d_{z^2} orbital is mixed with several ligand based orbitals in $[MoO(p\text{-}SC_6H_4CONHMe)_4]^-$, the energy difference between the d_{z^2} and the $d_{x^2-y^2}$ orbitals could not be quantified. In all cases, the composition of the HOMO (primarily Mo d_{xy}) is very similar suggesting that the geometry optimization primarily affects the virtual orbitals in this system. Thus, the ground state calculations on X-ray derived geometry provide a reasonable approach for understanding the properties of these orbitals.

The highest occupied molecular orbitals of $[MoO(SPh)_4]^-$ and $[MoO(p\text{-}SC_6H_4CONHMe)_4]^-$ are presented in Figure 7 while their compositions are listed in Tables 3 and S1. In both cases, the HOMO orbitals are primarily d_{xy} in character with contributions from sulfur pseudo-σ orbitals. Four sulfur π orbitals with e, a, and b symmetries appeared below the HOMO. The sulfur pseudo-σ orbitals have lower energy as compared to the sulfur π orbitals. This orbital description is analoguous to those describing the ground state DFT calculations on a truncated model, $[MoO(SMe)_4]^-$.[49] Like other square-pyramidal oxo−molybdenum complexes, the terminal oxo-group strongly destabilizes the d_{z^2} orbital

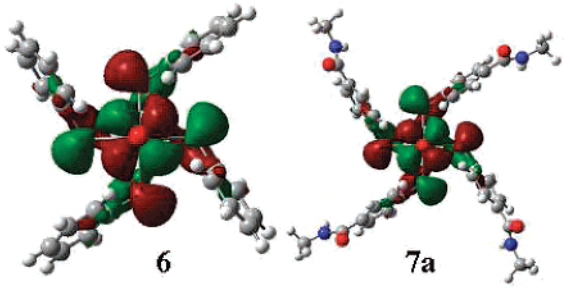

Figure 7. Pictorial representation of the HOMO for **6** and **7a**.

making it higher in energy than other d orbitals. Strong σ interactions between the equatorial sulfur and molybdenum $d_{x^2-y^2}$ orbital lead to a displacement of the molybdenum atom from the S_4 plane. The $d_{x^2-y^2}$ orbital moves away from the Mo−S vectors decreasing the $S^{\sigma}-Mo(d_{x^2-y^2})$ interaction, which results in stabilization of the $d_{x^2-y^2}$ orbital. The terminal oxo group contributes to the degenerate $d_{xz,yz}$ orbitals, i.e., the LUMOs for both $[MoO(SPh)_4]^-$ and $[MoO(p\text{-}SC_6H_4CONHMe)_4]^-$. The contribution of the Mo d_{xy} to the HOMO orbital is similar in $[MoO(SMe)_4]^-$, $[MoO(SPh)_4]^-$, and $[MoO(p\text{-}SC_6H_4CONHMe)_4]^-$; however, the presence of aromatic rings in the later complexes decreases the contribution from the sulfur atoms to the HOMO.

In recent years, time-dependent density functional theory (TDDFT) has become a popular tool for calculating the vertical excitation energies in inorganic and organometallic complexes. A few examples of calculations on closed-shell molybdenum-containing systems have been reported in the literature.[55] Recently, a detailed investigation of the influence of the basis set, exchange-correlation functional, and starting geometries on the vertical excitation energies in an open-shell $[MoOCl_4]^-$ complex has been conducted.[34] In the present case, TDDFT calculations on **6** and **7a** have been carried out. The results are presented in Table 4. In each case, four ligand-to-metal charge transfer (two of them are degenerate) and two predominantly d−d transitions (one of

Table 3. Calculated Orbital Composition for **6** and **7a** Using Experimental Geometry

	ROB3LYP[a]										UB3LYP				
	$[MoO(SPh)_4]^-$, $[MoO(p\text{-}SC_6H_4CONHMe)_4]^-$					$[MoO(SPh)_4]^-$ [b]					$[MoO(p\text{-}SC_6H_4CONHMe)_4]^-$ [b]				
		orbital composition					orbital composition					orbital composition			
	E, eV	Mo	Mo(d)	O	S	*E*, eV	Mo	Mo(d)	O	S	*E*, eV	Mo	Mo(d)	O	S
7e	−3.642;	13.6;	4.8;	0.6;	60.3;	−3.664;	14.1;	5.0;	0.7;	59.5;	−4.225;	13.9;	4.8;	0.7;	58.3;
	−4.203	13.5	4.7	0.6	59.2	−3.635	13.1	4.6	0.5	61.0	−4.196	13.0	4.5	0.5	59.9
7b	−3.146;	27.0;	27.0;	0.0;	40.4;	−3.797;	66.9;	66.9;	0.0;	11.5;	−4.372;	66.3;	66.3;	0.0;	10.7;
	−3.722	25.9	25.9	0.0	39.3	−3.002	27.3	27.3	0.0	40.2	−3.582	26.2	26.2	0.0	39.1
9a	−3.277;	9.1;	0.3;	1.5;	64.1;	−3.367;	8.9;	0.2;	1.4;	62.8;	−3.93;	8.5;	0.2;	1.4;	60.3;
	−3.844	8.7	0.3	1.5	61.9	−3.228	9.3	0.3	1.5	64.6	−3.798	8.9	0.3	1.5	62.5
8e	−2.96;	4.2;	3.9;	5.1;	61.6;	−3.054;	3.7	3.5;	5.3;	61.0;	−3.624;	3.5;	3.2;	5.1;	59.2;
	−3.534	3.8	3.6	5.0	59.8	−2.911	4.5	4.2	5.0	61.7	−3.487	4.2	3.9	4.8	60.0
8b[c]	−0.881;	74.1;	74.1;	0.0;	18.0;	−2.156;	35.5;	35.5;	0.0;	45.3;	−2.741;	34.7;	34.7;	0.0;	43.6;
	−1.272	73.6	73.6	0.0	17.2	−0.091	66.2	66.2	0.0	19.8	−0.674	64.5	64.5	0.0	18.4
9e	1.300;	56.9;	56.8;	10.8;	11.3;	1.225;	57.1;	57.0;	11.3;	11.7;	0.576;	52.7;	52.7;	10.7;	9.9;
	0.640	51.8	51.7	10.0	9.3	1.432	55.9	55.8	10.1	10.7	0.75	49.0	48.9	9.1	8.3
9b	2.081;	32.0;	32.0;	0.0;	20.8;	2.048;	33.5;	33.5;	0.0;	66.5;	1.225;	22.5;	22.5;	0.0;	13.2;
	1.247	21.1	21.1	0.0	11.7	2.143	29.0	29.0	0.0	17.4	1.297	19.3	19.3	0.0	10.3
10a	2.227;	39.9;	15.7;	3.6;	11.1;	2.199;	43.5;	18.2;	4.3;	12.2;	1.239;	11.5;	3.6;	0.9;	3.1;
	1.243	10.9	3.3	0.8	3.0	2.269	33.4	11.3	2.6	9.1	1.252	10.1	2.8	0.6	2.9

[a] Top line for $[MoO(SPh)_4]^-$ and the bottom line for $[MoO(p\text{-}SC_6H_4CONHMe)_4]^-$. [b] The α and the β orbitals are presented sequentially. [c] SOMO or α HOMO orbital.

Scheme 3

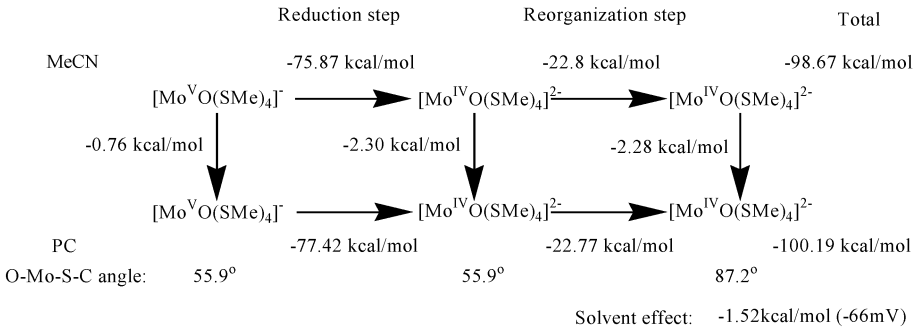

Table 4. Vertical Transition Energies for $[MoO(SPh)_4]^-$ and $[MoO(p\text{-}SC_6H_4CONHCH_3)_4]^-$ Calculated by TDDFT Approach

band	transition description	polarization	E, cm^{-1}	f
	$[MoO(SPh)_4]^-$			
1	137(b)$\beta \rightarrow$ 140(b)β (100%)	z	14948	0.0000
2	138(e)$\beta \rightarrow$ 140(b)β (92%)	x,y	15198	0.0370
3	139(e)$\beta \rightarrow$ 140(b)β (92%)	x,y	15198	0.0370
4	140(b)$\alpha \rightarrow$ 142(e)α (76%)	x,y	16667	0.0288
5	140(b)$\alpha \rightarrow$ 141(e)α (76%)	x,y	16667	0.0288
6	136(a)$\beta \rightarrow$ 140(b)β (96%)	forbidden	17825	0.0000
7	134(e)$\beta \rightarrow$ 140(b)β (17%); 135(e)$\beta \rightarrow$ 140(b)β (81%)	x,y	19685	0.0021
8	134(e)$\beta \rightarrow$ 140(b)β (81%); 135(e)$\beta \rightarrow$ 140(b)β (17%)	x,y	19685	0.0021
9	140(b)$\alpha \rightarrow$ 143(b)α (44%); 138(e)$\beta \rightarrow$ 141(e)β (10%); 139(e)$\beta \rightarrow$ 142(e)β (10%)	z	23809	0.0002
	$[MoO(p\text{-}SC_6H_4CONHCH_3)_4]^-$			
1	197(b)$\beta \rightarrow$ 200(b)β (100%)	z	15049	0.0000
2	198(e)$\beta \rightarrow$ 200(b)β (91%)	x,y	15191	0.0455
3	199(e)$\beta \rightarrow$ 200(b)β (92%)	x,y	15191	0.0455
4	200(b)$\alpha \rightarrow$ 201(e)α (81%)	x,y	16605	0.0404
5	200(b)$\alpha \rightarrow$ 202(e)α (81%)	x,y	16605	0.0404
6	196(a)$\beta \rightarrow$ 200(b)β (96%)	forbidden	17790	0.0000
7	194(e)$\beta \rightarrow$ 200(b)β (11%); 195(e)$\beta \rightarrow$ 200(b)β (86%)	x,y	19608	0.0032
8	194(e)$\beta \rightarrow$ 200(b)β (86%); 195(e)$\beta \rightarrow$ 200(b)β (11%)	x,y	19608	0.0032
9	200(b)$\alpha \rightarrow$ 203(b)α (48%); 198(e)$\beta \rightarrow$ 201(e)β (9%); 199(e)$\beta \rightarrow$ 202(e)β (9%)	z	23402	0.0005

which is degenerate) have been calculated in the low energy region. All calculated band positions are in the good agreement with the experimental assignments given for $[MoO(SPh)_4]^-$ and related complexes on the basis of UV−vis and MCD spectroscopies and ground state DFT calculations.[49,50,48] The calculated oscillator strengths are also in good agreement with the experimental data except the first formal d−d transition. Here, because of the spin-polarization for the α orbital set,[56] the calculated intensity is probably overestimated. More importantly, despite the difference between electronic structure of the para-substituents in these two compounds (−H versus $-CONHCH_3$), the calculated vertical excitation energies are very similar to each other

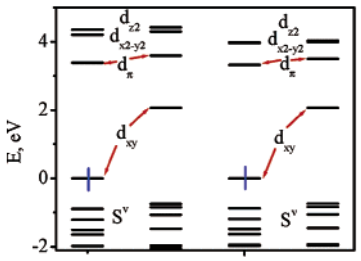

Figure 8. Molecular orbital diagrams for **6** (left) and **7a** (right).

with a typical deviation ∼50−100 cm^{-1}. Thus, the stabilization of the occupied orbitals in **7a** does not change the interorbital energy difference that results in very similar vertical excitation energies. Indeed, the calculated relative orbital energies for complexes **6** and **7a** at unrestricted open shell formalism are very close to each other (Figure 8).

5. The Solvent Effect. In order to understand the nature of the solvent effect observed in the reduction potentials of complexes **6** and **7a**−**c**, we have calculated the energy of the molecule under a variety of conditions (Scheme 3). The calculations for Scheme 3 were performed on reduced-size models, $[MoO(SMe)_4]^{n-}$ ($n = 1, 2$). Each reduction processes of Scheme 3 in specific solvent can be presented as a sum of two individual steps. The first step is the addition of one electron to the molybdenum(V) center keeping the same geometry. In the second step, the molybdenum(IV) complex is allowed to settle into a lower energy conformation. The calculations show that the primary difference in the two Mo(IV) geometries is in the O−Mo−S−C torsion angle (∼56° for Mo^V and ∼87° for Mo^{IV}). Scheme 3 fits well with the results obtained from the digital simulations of cyclic voltammograms using an EC mechanism, where the first step is the Mo(V) to Mo(IV) electron transfer step and the second chemical transformation step can be referred to the reorganization step in the Mo(IV) state. The energy of the molecule associated with both the steps was calculated in acetonitrile as well as propylene carbonate. The geometric rearrangement is under investigation and will be discussed elsewhere.[57] The solvent effect for the individual steps was calculated as the difference between the energy of the same compound in different solvents, while the solvent effect for the complete reduction process was taken as the addition of the individual components and then taking a difference. The calculated solvent effect ∼ −66 mV for the model system is comparable

(55) Broclawik, E.; Borowski, T. *Chem. Phys. Lett.* **2001**, *339*, 433−437. Adamo, C.; Barone, V. *Theor. Chem. Acc.* **2000**, *105*, 169−172. Wakamatsu, K.; Nishimoto, K.; Shibahara, T. *Inorg. Chem. Commun.* **2000**, *3*, 677−679. Rosa, A.; Baerends, E. J.; van Gisbergen, S. J. A.; van Lenthe, E.; Groeneveld, J. A.; Snijders, J. G. *J. Am. Chem. Soc.* **1999**, *121*, 10356−10365.

(56) Li, J.; Noodleman, L.; Case, D. A. In *Inorganic Electronic Structure and Spectroscopy*; Solomon, E. I., Lever, A. B. P., Eds.; Wiley: New York, NY, 1999; pp 661−724.

(57) Sengar, R. S.; Basu, P. Unpublished results.

to the experimentally observed values for complexes **6** and **7a**−**c** (from −18 to −87 mV). The calculated energy for the reduction step has been found to the dominant factor in Scheme 3 (∼76 kcal/mol), with a significant contribution from the reorganization energy (∼23 kcal/mol). Interestingly, models for molybdenum(V) and molybdenum(IV) states are more stable in propylene carbonate (dielectric constant 64.4), with the stability of the Mo(IV) state is three times higher.

Discussion

1. Thermodynamic Consideration. A fundamental goal of the present investigation is to delineate the factors that contribute to the reduction potential of oxo−molybdenum centers. Although this is a complex issue, understanding the factors that influence the redox potentials can provide insight into enzymatic function. It has been reported that the reduction potential (E_0) of an active site in a metalloenzyme can be described with the help of eq 1, where 4.5 corrects the potential to that of NHE, IE is the ionization energy, and U is a solvation term.[51]

$$E_0 = \mathrm{IE} + U - 4.5 \qquad (1)$$

The ionization energy term is dependent on the electronic structure, i.e., the energy of the redox orbital. Similarly, the energy of the redox orbital is dependent on the effective nuclear charge, and the geometry of the active site. The solvation term is composed of factors such as specific interaction with charged residues, the H-bonding that can preferentially stabilize either the reduced or oxidized state of the metal, and the general control of the dielectric relative to the aqueous solution.[58]

One possible way to change the energy of the redox orbital is by imposing distortion at the metal center. It has been demonstrated that a sterically demanding ligand, e.g., bis-(thiophenol) imposes a distortion at the oxomolybdenum-(V) center resulting in the change of the energy of the redox orbital and hence the reduction potential.[50] Even for relatively rigid iron−porphyrinate molecules, 2-Me-imidazoles as axial ligands rather than the *N*-Me-imidazole change the ground state electronic structure. This change is manifested in their EPR spectra.[59] In the present system, if the ligand bulk can effectively reduce the local symmetry from C_4, the reduced symmetry should be manifested in their EPR spectra. The axial EPR spectra, with similar *g*-values, clearly demonstrate that the local symmetry is unperturbed even with bulkier ligands. As mentioned, optical spectroscopy is a sensitive probe for evaluating subtle distortion at the metal center such as those due to a difference in the torsion angle. In the present case, the low energy band offers discerning features of distortion that can be evaluated in MCD spectra. A detailed magnetic circular dichroism investigation, reported elsewhere[48] that shows little change in the band positions, also supports this conclusion; i.e., in the +5 oxidation state the geometry of the metal center is very similar in these molecules. Interestingly, the solid-state structures of $[MoO(SAr)_4]^{2-}$ complexes differ from the $[MoO(SAr)_4]^{-}$ structures with opposite phenyl rings, changing conformation away from the propeller type arrangements, thereby lowering gross symmetry of the molecule.[22]

The electronic contribution was further evaluated by electronic structure calculations at the DFT level. While the electronic structures of **6** and **7a** can be directly compared, it is inferred for **7b** and **7c** from the calculations on respective ligands. The calculated energy difference between the SOMO (in the case of restricted open formalism) or β-LUMO (in the case of unrestricted formalism) orbitals of complexes **6** and **7a** is at least 0.391 eV, indicating that the electron-withdrawing $-CONHCH_3$ group stabilizes the occupied orbitals in **7a** compared to **6** (Table 3). The DFT calculations on dendritic molecules are computationally expensive and have not been attempted, the electronic term could not be directly compared for complexes **7b** and **7c** as in the case of **6** and **7a**. However, the following two observations can provide information about the energy of this orbital. First, the computed Mulliken charges on sulfur for the dendritic ligands are similar (−0.269, −0.295, and −0.290 au for *p*-$HSC_6H_4CONHMe$, **5b**, and **5c**, respectively) and differ significantly from that calculated for HSPh (−0.18 au).[39] The Mulliken charge on sulfur atoms has been shown to vary linearly with the reduction potentials in oxo−molybdenum-(V) ene-dithiolate complexes.[60] However, in the present case the charges on the sulfur atoms do not correlate as well with the experimental reduction potentials of **6** and **7a**−**c**, and if the relation derived for the ene-dithiolate is used, a ∼4 mV difference in the reduction potential between **7a** and **7b** is predicted. Furthermore, the Mo^{V}/Mo^{IV} reduction potentials of substituted thiophenolato complexes of general formula $[MoO(SAr)_4]^{-}$ exhibit a modest correlation with the Hammett (σ_p^{+}) constants,[46] and inclusion of the dendrimer data does not improve the correlation significantly. Taken together, it is apparent that while there is a significant change in the electronic structure (imposed by the ligand electronic environment) from **6** to **7a**, such a change cannot account completely for the variation in the redox potential from **7a** to **7c**.

All compounds are easier to reduce in propylene carbonate, whose dielectric constant is considerably larger (64.4) than that of MeCN (37). We believe that this stabilization is purely electrostatic in origin, with the larger dielectric constant in propylene carbonate preferentially stabilizing the Mo(IV) state. Interestingly, complex **7a** is easier to reduce than complex **7c**. This behavior suggests a destabilization due to the dendritic architecture in **7c**. Such a trend was also observed in other redox-active dendritic systems. In these molecules, the Mo═O unit provides a direction of the dipole, and organization of the solvent molecules with respect to this dipole can influence the reduction potential. The IPCM calculations on a simplified model suggest that the energy for the reduced form is ∼76 kcal/mol more stable in MeCN than the corresponding Mo(V) complex. This stabilization

(58) Kassner, R. J.; Yang, W. *J. Am. Chem. Soc.* **1977**, *99*, 4351−4355.
(59) Basu, P.; Raitsimring, A. M.; Enemark, J. H.; Walker, F. A. *Inorg. Chem.* **1997**, *36*, 1088−1094.
(60) Helton, M. E.; Gruhn, N. E.; McNaughton, R. L.; Kirk, M. L. *Inorg. Chem.* **2000**, *39*, 2273−2278.

is more in propylene carbonate that has a higher dielectric constant. Along with the stabilization of the Mo(IV) state, the energy associated with the relaxation in the O−Mo−S−C torsion angle is also substantial, although less than the reduction step. This geometric rearrangement has an important kinetic consideration that is discussed later.

In DMF, the situation is quite different. Here, the dendritic effect upon the reduction potential of complexes **7a**−**c** is small (Table 1). This is surprising, because it is expected that an increase in the dendrimer size should more effectively encapsulate the redox-active molybdenum atom from the solvent molecules. The observed behavior can be explained by taking into consideration the possibility of the hydrogen bond formation between amide proton of the **7a**−**c** complexes and the DMF oxygen atom.[61] Indeed, among the solvents tested, DMF is more effective in forming hydrogen bonds and thus providing the solvent specific interaction. This interaction leads to a smaller separation in the reduction potentials for compounds **7a**−**c** and contributes to the shift of the reduction potentials of **7a**−**c** by ∼100 mV than in MeCN. Interestingly, the reduction potential of **6** is shifted only 60 mV in DMF. The larger shift in complexes **7a**−**c** is clearly indicative of solvent specific interactions. Hydrogen bonding would increase the partial negative charge on the nitrogen atom, effectively enhancing the electron donating properties and making the reduction more difficult. Then, why do we observe a 50 mV shift in reduction potential in DMF (relative to MeCN) for compound **6**, when both DMF and MeCN have similar dielectric constants? We believe that the explanation lies in the donor numbers for these solvents. Among the three solvents, DMF has the highest donor number, which should make ionic complexes less ion paired. The oxo−molybdenum complexes, isolated as salts of PPh_4, are more "ion paired" in MeCN and propylene carbonate, while they are more ionized in DMF. Thus, the shift in the reduction potential for **6** from MeCN to DMF may reflect the difficulty in reducing a monoanionic species to a dianionic species.

2. Kinetic Consideration. Molecules **7a**−**c** display an increasingly larger peak-to-peak separation potential difference between the current maxima of the reduction and return oxidation waves (ΔE), indicative of increasing kinetic difficulty of reduction and oxidation processes. The electrochemical data suggest that increasing the steric bulk of the ligand far from the metal center induces sluggish redox chemistry, a behavior exhibited by other encapsulated redox-active metal centers.[18] Certainly, such an insulating effect can be operative in this system. In addition, it is possible that the reorganization energy, detailed in Marcus theory, can also contribute to the observed peak-to-peak separation. This would mean that significant differences exist within these molecules in the Mo(IV) state. We have already mentioned that upon reduction the reduced species relaxes its geometry by increasing the O−Mo−S−C torsion angle. It has been demonstrated that the Mo(IV) complexes of *o*-substituted thiolphenolato ligands are in an equilibrium between conformers of different symmetry.[44] At lower temperatures, all four amide groups are placed syn to the Mo═O vector, while at higher temperatures two of the amide groups point away from the Mo═O group lowering the symmetry. Thus, at high temperature, a low symmetry conformer is preferred while at lower temperatures, a high symmetry conformation is favored. Such a stereochemical rearrangement could also be operating in the dendritic system. Because stereochemical rearrangements in dendritic ligands would require more energy, it can attenuate the rate of electron transfer.

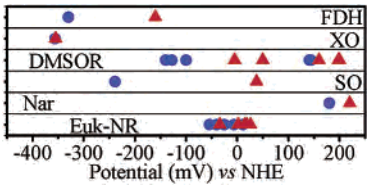

Figure 9. Reduction potential of selected molybdenum enzymes at pH ∼ 7: circles (●) represent the Mo(VI/V) couple, and triangles (▲) represent Mo(V/IV) couple.

3. Relation to Enzymes. The reduction potentials are exquisitely sensitive to applied conditions such as temperature, pH, and source. Figure 9 shows the reduction potentials of Mo centers of mononuclear molybdoenzymes at pH 7. Note that the Mo(VI/V) and Mo(V/IV) potentials of *E. coli* NarG are 220 and 180 mV, respectively, but for DMSOR, isolated from the same organism, they are −75 and −90 mV. These two enzymes have the same Mo centers, yet the redox potentials are ∼300 mV apart. Another interesting feature is that, with the exception of chicken liver sulfite oxidase, the Mo(VI/V) and Mo(V/IV) couples are separated by only 15−20 mV.[62] In contrast, the redox potentials of discrete inorganic complexes are often ∼1500 mV apart.[63]

In all of crystal structures, the Mo centers have been found to be encapsulated inside the protein matrix (typically ∼10−15 Å from the surface) and are not exposed to the solvent (Figure 10). In general, there is a channel associated with the Mo center for substrate entrance and product release. This feature is in contrast to other electron transfer proteins such as cytochrome b,[64] plastocyanin,[65] or ferredoxin[66] where either the metal ion or a part of the coordinating ligand frame is exposed to the exterior surface. Furthermore, the crystal structure of the substrate bound form of DMSOR demonstrates that the molybdenum is not exposed to the catalytic pocket. This is interesting because for other protein-encapsulated metal centers, such as the Zn in carbonic anhydrase, the metal is exposed to the catalytic pocket. We hypothesize that the microenvironment created by the protein backbone can modulate the reduction potential.

(61) Stone, D. L.; Smith, D. K.; McGrail, P. T. *J. Am. Chem. Soc*. **2002**, *124*, 856−864.

(62) Spence, J. T.; Kipke, C. A.; Enemark, J. H.; Sunde, R. A. *Inorg. Chem.* **1991**, *30*, 3011−3015.

(63) Graff, J. N.; McElhaney, A. E.; Basu, P.; Gruhn, N. E.; Chang, C.-S. J.; Enemark, J. H. *Inorg. Chem.* **2002**, *41*, 2642−2647.

(64) Rodriguez-Maranon, M. J.; Qiu, F.; Stark, R. E.; White, S. P.; Zhang, X.; Foundling, S. I.; Rodriguez, V.; Schilling, C. L.; Bunce, R. A.; Rivera, M. *Biochemistry* **1996**, *35*, 16378−16390.

(65) Yafeng, X.; Mats, O.; Orjan, H.; Simon, Y. *Protein Sci*. **1998**, *7*, 2099−2105.

(66) Tsukihara, T.; Fukuyama, K.; Mizushima, M.; Harioka, T.; Kusunoki, M.; Katsube, Y.; Hase, T.; Matsubara, H. *J. Mol. Biol.* **1990**, *216*, 399−410.

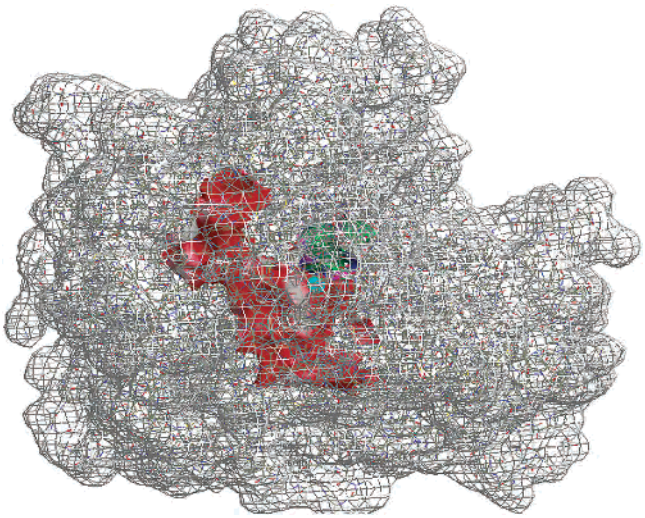

Figure 10. The encapsulated Mo-center derived from the crystal structure of DMSO reductases (reference 7).

In this regard, dendritic architecture has been thought to generate microenvironments. It has been argued that branched dendritic shells can generate microenvironments that can modify the properties of the functional cores. While such microenvironments can be used for generating new functional materials with modified cores, this emulates the microenvironments created by protein superstructures. Although only the first generation dendritic ligands were used here, the mononuclear metal core has four branching points originating from four thiophenolato ligands, which when compared to the bulk, creates a different environment at the metal center. As mentioned, in all mononuclear molybdoenzymes, the molybdenum center is deeply buried, and intense hydrogen bonding networks create microenvironments differing from that of the bulk. The present molecules provide the first attempt at topological modeling of pterin-containing mononuclear molybdoenzymatic centers.

The dielectric control of the redox potential in heme proteins and ferredoxins has been discussed using synthetic molecules. As a model for globular heme proteins, the Diederich group has reported that the redox potential of a second generation dendritic iron porphyrinate molecule is 420 mV more positive than the corresponding first generation complex in CH_2Cl_2, whereas in water the shift is only 12 mV.[67] This study suggests that the solvent dielectric can play an important role in modulating the redox potential through its effects on the ligand backbone. Gorman et al. have observed that the reduction of the encapsulated 4Fe4S clusters become progressively more difficult, both thermodynamically and kinetically, as a function of dendrimer growth (i.e., the degree of encapsulation).[68] These studies clearly indicate that encapsulation has a significant effect on the redox behavior of iron porphyrins and 4Fe4S clusters. Similar conclusions were also drawn from studies of encapsulated abiological cores such as ferrocene.[18] Thus, it is provocative to suggest that protein structure imposed microenvironments at the metal center may be a general feature in many metalloenzymes, and dielectric control of such center may be a general mode of operation in nature.

Concluding Remarks

In conclusion, we have discussed the synthetic route to a novel architecture for investigating the encapsulated oxo−molybdenum(V) centers. The effect of the encapsulation on the redox properties of the $[Mo^{V}OS_4]^-$ core without imposing significant distortion is demonstrated. The electronic structure of oxo−Mo(V) centers, calculated by a DFT method, shows a very similar composition of the redox orbital. Furthermore, the redox chemistry of the molybdenum complexes was investigated in three different solvents with varying dielectric constants and donor numbers. In all solvents, the dendritic Mo complexes show sluggish electrochemistry. The NH hydrogen appears to support hydrogen bond formation in DMF, while the reduced state is better stabilized in propylene carbonate. Thus, the influence of solvent on redox potential without significantly altering the geometric contribution to electronic structure is demonstrated.

Acknowledgment. We are grateful to Professor Michael Hendrich for recording the EPR spectra, and greatly appreciate Dr. R. Belosludov's assistance in TDDFT computation. We also thank Professors F.A. Schultz, M. Rivera, J. Madura, and M. L. Kirk for numerous helpful discussions, and Dr. Sujit Mondal for preliminary experiments. Financial support from Research Corporation and the National Institutes of Health (GM 6155501) is gratefully acknowledged.

Supporting Information Available: UV−vis spectra of **6** in different solvents (Figures S1) and the linear relations between the square root of scan rate and peak current (Figure S2). The orbital composition of **6** and **7a** calculated from optimized geometries are listed in Table S1. Optimized coordinates, energies, and frequencies for **6**, **7a**, and $[MoO(SMe)_4]^{n-}$ ($n = 1,2$). This material is available free of charge via the Internet at http://pubs.acs.org.

IC034821R

(67) Weyermann, P.; Gisselbrecht, J.-P.; Boudon, C.; Diederich, F.; Gross, M. *Angew. Chem., Int. Ed.* **1999**, *38*, 3215−3219. Dandliker, P. J.; Diederich, F.; Gisselbrecht, J.-P.; Louati, A.; Gross, M. *Angew. Chem., Int. Ed. Engl.* **1995**, *34*, 2725−2728. Dandliker, P. J.; Diederich, F.; Zingg, A.; Gisselbrecht, J.-P.; Gross, M.; Louati, A.; Sanford, E. *Helv. Chim. Acta* **1997**, *80*, 1773−1801.

(68) Gorman, C. B.; Parkhurst, B. L.; Su, W. Y.; Chen, K.-Y. *J. Am. Chem. Soc.* **1997**, *119*, 1141−1142.